www.czasopisma.pan.pl PAN POLSKA AKADEMIA NAUK www.journals.pan.pl

A R C H I V E S O F M E T A L L U R G Y A N D M A T E R I A L S

Volume 59 2014 Issue 4

DOI: 10.2478/amm-2014-0247

J. KONSTANTY*, A. ROMANSKI*

NUMERICAL ANALYSIS OF DIAMOND RETENTION IN COBALT AND A COPPER-BASE ALLOY

ANALIZA NUMERYCZNA RETENCJI KRYSZTAŁU DIAMENTU W KOBALCIE I STOPIE MIEDZI

Why cobalt outperforms other matrix materials in its capacity for diamond retention in cutting tools is considered. To this end diamond loading conditions were modelled to establish the magnitude of stress and strain in the matrix surrounding a working diamond crystal. Only at 315 N did the contact force in Co result in plastic strain of 4-8%, which has a destructive influence on diamond retention. The strain field generated in a poorly performing Cu-40%Co-6%Sn matrix under a load of 190 N closely resembled that generated by 315 N in Co. It is postulated that diamond retention is related to the yield strength and work hardening characteristics of the metallic matrix.

Keywords: matrix; wear; stress concentration; residual stress; finite element

W artykule przedstawiono analizę czynników decydujących o bardzo dobrych własnościach retencyjnych kobaltu w odniesieniu do kryształów diamentu w spiekanych materiałach narzędziowych. W tym celu przygotowano komputerowy model kryształu diamentu osadzonego w osnowie i poddanego działaniu zewnętrznego obciążenia dla ustalenia wielkości naprężeń i odkształceń pojawiających się w osnowie. Stwierdzono, że siła 315 N działająca na diament umieszczony w kobalcie powoduje odkształcenie plastyczne osnowy w zakresie 4-8%, co ma negatywny wpływ na retencję. W przypadku stopu Cu-40%Co-6%Sn podobne wartości odkształceń zaobserwowano pod działaniem siły 190 N. Na podstawie otrzymanych wyników symulacji komputerowych można stwierdzić, że własności retencyjne materiału osnowy uzależnione są od jego granicy plastyczności oraz zdolności do umocnienia wywołanego odkształceniem plastycznym.

1. Introduction

Various kinds of granite, dense refractories and fused ceramics are wet sawn in many passes with a reciprocating movement of a segmented circular saw blade, which alternately operates in the up-cutting and down-cutting modes (Fig. 1).

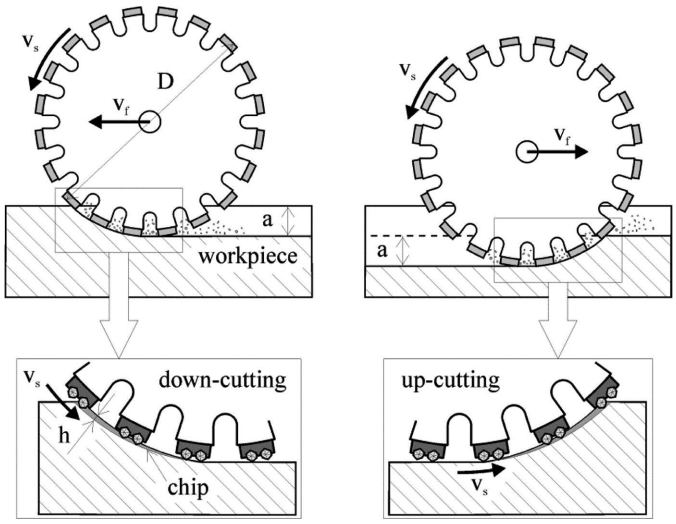

Fig. 1. Kinematic diagram of circular sawing

The depth of cut (a) usually ranges between 0.4 and 20 mm, whereas the feed rate (v_f) is adjusted to the saw blade characteristics, machine rigidity and power, and tool life requirements. Thus cutting rates ($a \cdot v_f$) vary from 300 to 600 cm^2/min under standard and heavy-duty conditions, respectively.

In down-cutting, each working diamond crystal penetrates into the workpiece to full depth when coming in contact with it, whereas in up-cutting, diamonds gradually increase the depth of penetration to achieve the maximum value while leaving the cutting zone. Consequently, the diamond breakdown is facilitated by downward rotation of the blade that, by its nature, creates pulsing impact forces acting on crystals which enter the cutting zone. Their magnitude depends on the maximum chip thickness (h_{max}) approximated as [1]

$$h_{max} \approx \frac{v_f \cdot a}{v_s \cdot C \cdot w} \cdot \sqrt{\frac{1}{a \cdot D} - \frac{1}{D^2}} \tag{1}$$

where C and w stand for the number of diamonds per unit surface and the average width of diamonds, respectively.

The failure of a diamond crystal is governed in a complex manner by its shape, orientation and ability to withstand impact forces, the magnitude of mechanical and thermal loading,

* AGH-UNIVERSITY OF SCIENCE AND TECHNOLOGY, FACULTY OF METALS ENGINEERING AND INDUSTRIAL COMPUTER SCIENCE, AL. A. MICKIEWICZA 30, 30-059 KRAKÓW, POLAND

and the matrix retention properties. With blocky and robust crystals (Fig. 2), used for the most demanding sawing tasks, the cutting conditions must be carefully chosen in order to facilitate their controlled micro-fracturing. Otherwise, due to insufficient diamond penetration depths (h_{max}), excessive friction leads to cutting point blunting (steps I and II in Fig. 3).

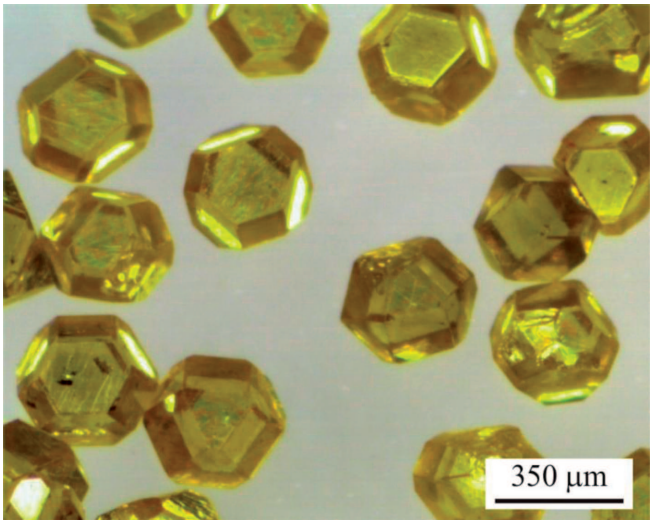

Fig. 2. High grade synthetic diamond

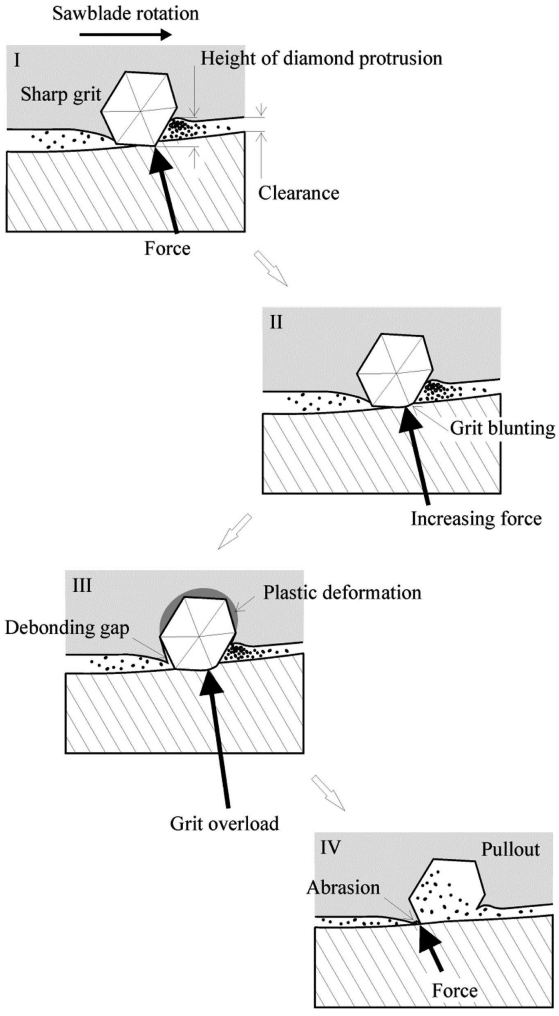

Fig. 3. Diamond pullout-controlled wear progression in circular sawing

This results in high forces oriented 80-85° normal to the stone surface [2], which, being transmitted to the matrix, may cause its plastic deformation (step III in Fig. 3). As each working diamond is subjected to cyclic loading, applied at 3-35 Hz intervals, depending on the blade diameter (0.3-3.5 m) and peripheral speed (25-35 m/s), each time the yield strength of the matrix is exceeded, the crystal seat slightly opens and thereby the hold on the diamond is being gradually destroyed. Finally, when pullout occurs, the trailing matrix ridge is immediately removed by harsh 2-body abrasion (step IV in Fig. 3). The wear rate then decays over time as clearance increases, and other forms of wear, such as 3-body abrasion and erosion, take over.

Both hardness and yield strength of the metallic matrix are still believed to give good indication of its diamond-holding ability. Such a simple approach to the problem of diamond retention neglects, however, at least three important facts. First, hardness tests involve relatively high plastic strain of between 5-12% [3]. Second, both hardness and yield strength are measured by means of static tests, whereas the diamond/matrix set-up is subjected to high frequency impact loading which may affect the yielding behaviour of the matrix. Although the load duration estimates are available [2], the actual stress regime cannot be quantified and it is difficult to precisely determine the strain rates involved. Third, a typical diamond cutting point maintains protrusion for around 30 000 impacts [2,4,5], which implies fatigue of the matrix.

In view of all these limitations, the diamond retention capacity of the matrix can be reliably estimated only in sawing tests by counting the number of diamonds and pullouts on the tool working face and calculating the proportion of the total number of diamonds to the total number of diamonds and pullouts. Such tests were previously carried out by the authors on class IV granite using 250 mm segmental saw blades which contained 40/50 US mesh premium grade diamond at 20 concentration (5 vol.%) and differed in the matrix material [6,7,8]. In addition to the number of diamonds and pullouts, the working face of the saw blades were also analysed for the height of diamond protrusion using an optical profiler.

The results are given in Table 1.

TABLE 1

Diamond crystal retention and protrusion [6,7,8]

Matrix	Total number of diamonds retained on saw blade [a]	Mean height of diamond protrusion [b] (μm)
Co	757 (71%)	70±5
Cu-40%Co-6%Sn	544 (49%)	56±5

[a] values in brackets represent the proportion of the total number of diamonds to the total number of diamonds and pullouts

[b] confidence intervals were estimated at 90% confidence level

2. Experimental procedure and results

2.1. Modelling the diamond/matrix setup

On the basis of previous works [9,10], the strain rate independent, 3D finite element analysis (FEA) was carried out for both the Co and Cu-40%Co-6%Sn matrix using ABAQUS

software. The stress/strain distribution field was studied for a single cubo-octahedral diamond crystal, having a morphology index τ =0.25 [11], which had been partially embedded in a metal matrix, as shown schematically in Fig. 4.

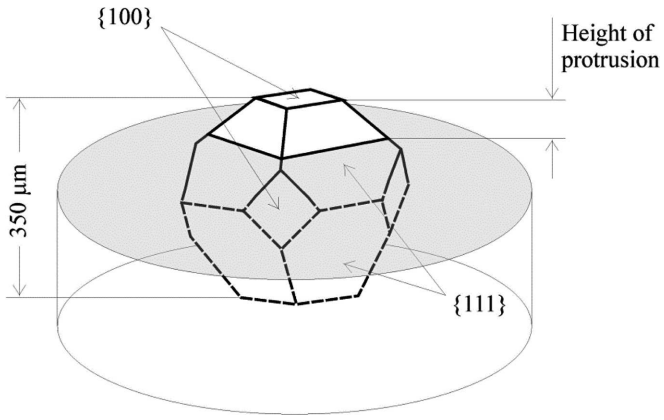

Fig. 4. Perfectly shaped diamond crystal partially embedded in a metal matrix

The diamond was meshed with 3456 linear hexahedral elements of type C3D8R, whereas the matrix was meshed with either 15924 or 12368 linear tetrahedral elements of type C3D4 for the crystal protrusion of 50 and 70 μm, respectively.

2.2. Modelling the cooling stress

During the cooling stage of the hot pressing cycle a stress field arises in the matrix surrounding each diamond crystal due to a mismatch between the thermal expansion coefficients. As the dependence of mechanical and thermal characteristics of the system components on temperature is unavailable, analytical prediction of the amount of plastic strain and strain hardening, and their effect on the magnitude of the residual stress presents difficulty. It has been, however, proved experimentally that the application of μ-Raman spectroscopy allows quantification of hydrostatic stress that sets up in diamonds partially embedded in cobalt during segment fabrication [12]. Therefore, to reproduce the stress/strain conditions in a hot pressed segment, the diamond/matrix setup was pre-stressed by simulated cooling from an unstressed condition, existing at a hypothetical T_u temperature, lower than the hot pressing temperature, to 293 K. The model of an elastic-plastic material was applied and experimental true stress-true strain curves of Co and Cu-40%Co-6%Sn were used as the input data. It was also assumed that the main mechanical and thermal characteristics of the experimental matrix materials and diamond were temperature independent within the cooling range.

The ABAQUS input data are presented in Table 2.

The variation in hydrostatic stress along the central axis of a diamond crystal protruding above the cobalt matrix was calculated for three values of T_u, arbitrarily chosen as 450, 500 and 550 K, and compared with the μ-Raman data taken from ref [12]. As in the μ-Raman measurements, the stress was calculated for crystal protrusion of 50 μm.

The analytical and experimental stress distribution curves are presented in Fig. 5.

TABLE 2
Mechanical and thermal properties of matrix materials [6,8,13] and diamond [14]

Matrix properties at 293 K	Co	Cu-40%Co-6%Sn	Diamond
0.2% offset yield strength (MPa)	640	360	–
Young's modulus (GPa)	202	138	1050
Poisson's ratio	0.3	0.3	0.2
Thermal expansion coefficient ($10^{-6}\cdot K^{-1}$)	13.8	18.4	1.5
Static coefficient of friction on diamond	0.1	0.1	–

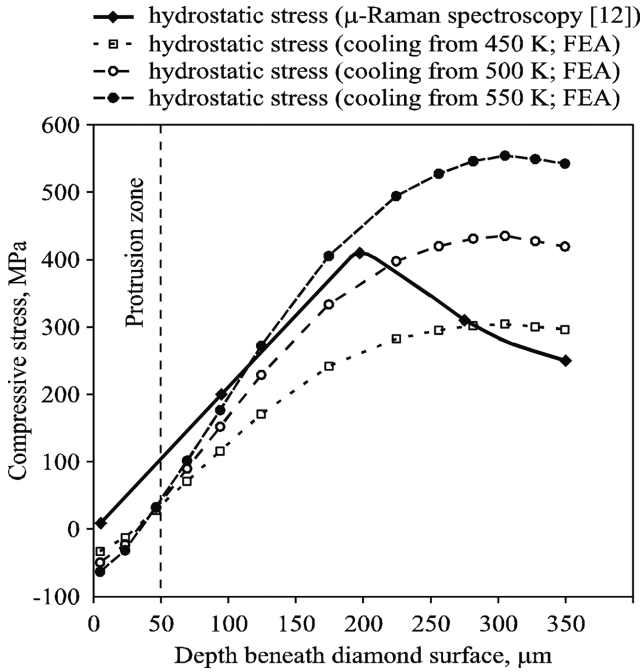

Fig. 5. Stress distribution curves in a diamond crystal protruding 50 μm above the cobalt matrix

As the surface stress in the μ-Raman spectroscopy measurements was normalised to zero [12], it is evident from Fig 5 that the hydrostatic stress distribution for T_u =500 K fits the experimental data within the depth range 0-200 μm. Interestingly, after cooling the system from 500 K the maximum von Misses stress reaches the yield strength of Co taken for the calculations (Table 2, Fig. 6a). Therefore, due to lack of μ-Raman spectroscopy data for the diamond/Cu-40%Co-6%Sn system, the T_u temperature was established by the yield strength criterion as 425 K (Fig. 6b).

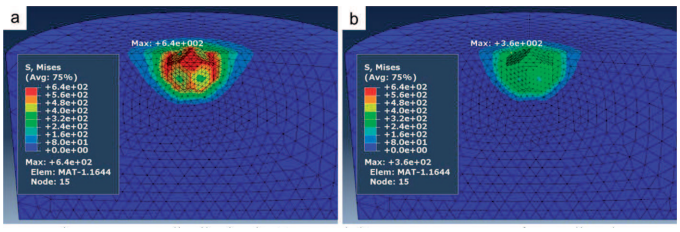

Fig. 6. Stress distribution in (a) Co and (b) Cu-40%Co-6%Sn after cooling the diamond/matrix setup from 500 and 425 K, respectively

2.3. Modelling the diamond loading conditions

In the next step the FEA was used to predict how the stress/strain field generated in the matrix during its consolidation reacts to an external force applied to the protruding diamond. Prior to loading, the diamond protrusion was increased to 70 μm to comply with the mean height of protrusion evaluated on the working face of real segments (Table 1). After pre-stressing by cooling from T_u, the diamond was loaded by a combination of pressure and a concentrated force as shown schematically in Fig. 7.

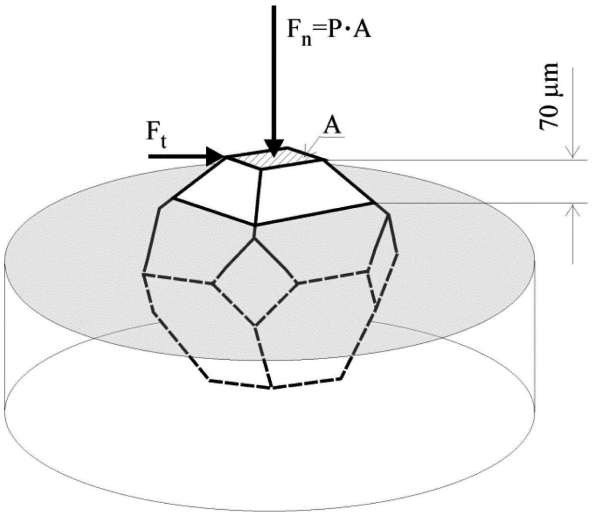

Fig. 7. Diamond loading scheme

The crystal loading conditions were inferred from the experimental data published in ref [15]. Detailed analysis of forces acting on a working saw blade indicates that the normal to tangential force ratio may vary between 4 and 11, depending on the cutting conditions [15]. As documented in Table 3, the tangential force per unit length of contact remains unaffected by the sawing conditions, whereas the normal force varies to a large extent.

TABLE 3

Results of sawing tests performed on class IV granite (adapted from ref [15]

Cutting rate $a \cdot v_f$ (cm^2/min)	Depth of cut a (mm)	Normal force per unit length of contact F_n(N/cm)	Tangential force per unit length of contact F_t (N/cm)	F_n/F_t [a]	h_{max} [b]
150	7.5	114	11	10.8 (5°)	1.00
300	10	68	11	6.3 (9°)	1.74
300	7.5	54	11	5.0 (11°)	2.00
450	15	48	12	4.2 (14°)	2.16

[a] values in brackets indicate the contact angle (φ) between the resultant force and its normal component

[b] relative values calculated using equation (1) and assuming $v_s \cdot C \cdot w = const$

Obviously the normal force per unit length of contact inversely correlates with h_{max}, which implies dulling of high grade diamonds at low penetration depths.

Experimental results obtained in sawing class IV granite by a single-crystal saw, fitted with force transducers, gave an average contact load of ~190 N per crystal cutting, a rate equivalent to 300 cm^2/min [2]. Such high contact loads, combined with the F_n figures from Table 3, imply that only one crystal per ~3 cm length of contact between the blade and granite is actually involved in cutting. This can be explained by two facts. First, at any moment only ~26% of crystals seen on the working face of a saw blade have sufficient height of protrusion to be involved in cutting [5], and second, in down-cutting the impact loading of the cutting crystal causes increased removal of workpiece material of a magnitude which prevents the trailing diamonds, or even segments, from engaging [16]. It should also be noted that high grade diamond crystals of 40/45 mesh size are sufficiently strong to withstand both static and dynamic forces exceeding 500 N [17].

In order to closely reproduce the conditions given in Table 3, the diamond crystal was loaded with a force of 130, 145, 190 and 315 N, angled versus its normal component at 14, 11, 9 and 5°, respectively.

The FEA results are shown in Table 4 and in Figs 8-11.

TABLE 4

Maximum von Mises stresses and plastic strains

Force (N)	Contact angle φ (deg)	Co		Cu-40%Co-6%Sn	
		Maximum stress (MPa)	Maximum strain (%)	Maximum stress (MPa)	Maximum strain (%)
130	14	769	1.42	517	4.24
145	11	797	1.83	530	4.96
190	9	851	3.39	543	8.15
315	5	963	8.38	–	–

3. Discussion

The ABAQUS software proved suitable for building a model of a cubo-octahedral diamond crystal partially embedded in a metal matrix, as well as for creating a digital representation of the stress/strain field arising both inside the diamond and in the diamond bearing matrix due to thermal contraction and mechanical loads during tool fabrication and use. Obviously the FEA approach does not account for variations in actual crystal shape, size and orientation, presence of other crystals within the analysed volume, sensitivity of the metal matrix to strain rate, its fatigue and mechanical properties at high strain rates, absorption of strain energy into the loaded crystal and strain transparency phenomena occurring at the crystal-matrix interface [2]. On the other hand, FEA is a simple means of calculating stresses and strains in the close proximity of a loaded diamond crystal which cannot be estimated otherwise.

The ABAQUS calculations demonstrated uneven distributions of stress and strain in the matrix surrounding the loaded crystal. The highest values were seen in areas (mesh nodes and elements) lying on the trailing side of the surface, or somewhat beneath it, and adjacent to sharp crystal edges (Figs 8 and 9).

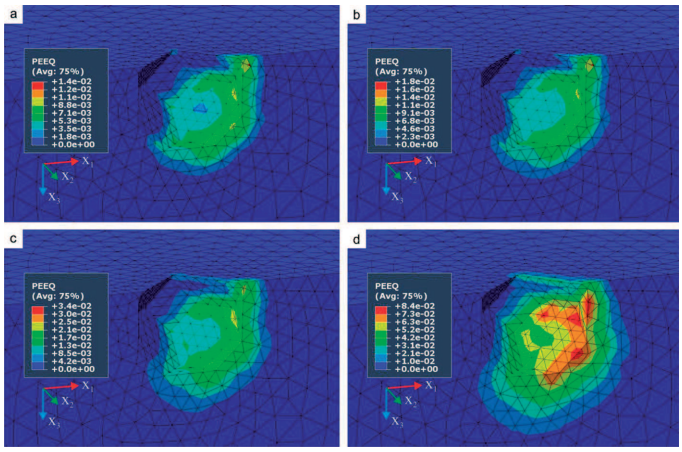

Fig. 8. Strain distributions in Co after loading through a protruding diamond with a force: (a) 130 N (φ =14°), (b) 145 N (φ =11°), (c) 190 N (φ =9°), (d) 315 N (φ =5°)

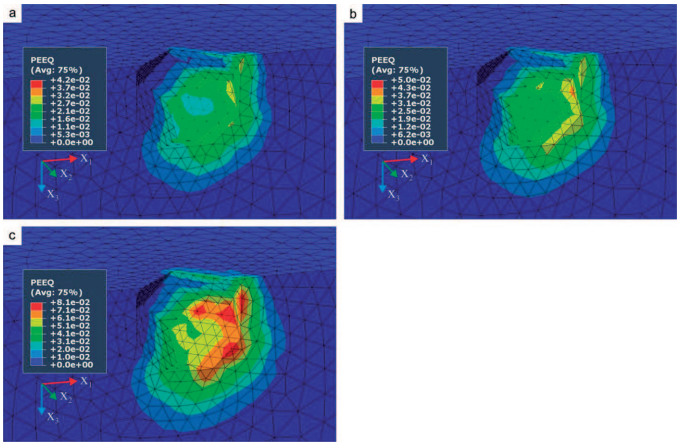

Fig. 9. Strain distribution in Cu-40%Co-6%Sn after loading through a protruding diamond with a force: (a) 130 N (φ =14°), (b) 145 N (φ =11°), (c) 190 N (φ =9°)

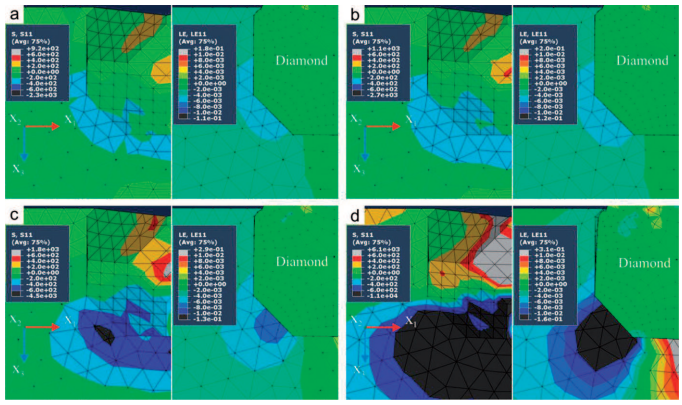

Fig. 10. Distributions of σ_{11} normal stress (left) and ε_{11} strain (right) components in Co loaded through a protruding diamond with a force: (a) 130 N (φ =14°), (b) 145 N (φ =11°), (c) 190 N (φ =9°), (d) 315 N (φ =5°)

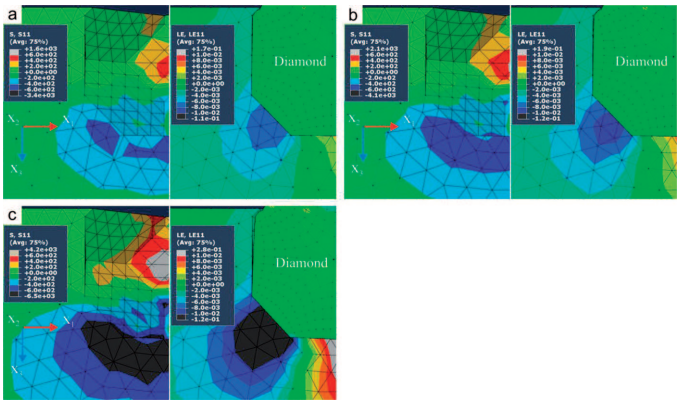

Fig. 11. Distributions of σ_{11} normal stress (left) and ε_{11} strain (right) components in Cu-40%Co-6%Sn loaded through a protruding diamond with a force: (a) 130 N (φ =14°), (b) 145 N (φ =11°), (c) 190 N (φ =9°)

This accounts for the location of debonding gaps (Fig. 3) seen along the back-edge of overloaded diamonds [6].

From an infinite number of force/contact angle combinations, the four experimentally derived examples (Table 3) were addressed in the analysis. As demonstrated in Table 3, high h_{max} values imply harsh impact loading of the working diamonds and mild loading conditions for the matrix. If the working part of the diamond remains rough, showing extensive micro-fracturing and no wear flatting, the cyclic loads remain bearable by the matrix.

Although for Co the maximum plastic strains for contact forces of 130 and 145 N were estimated at 1.4 and 1.8%, respectively (Table 4), detailed analysis of the strain distribution maps showed that only tiny volumes of the matrix had experienced plastic strain in excess of 1% (Figs 8a and 8b). The increase in the contact force to 190 N resulted in around two-fold increase in plastic deformation (Fig. 8c, Table 4), whereas, with further growth of the contact force to 315 N, the progressive build-up of plastic strain, to between 4 and 8%, could reach a critical volume, thus having a destructive influence on diamond retention (Fig. 8d). Interestingly the strain field generated in the poorly performing Cu-40%Co-6%Sn matrix under the load of 190 N (Fig. 9) closely resembled that brought about by 315 N in Co.

Detailed analysis of the σ_{11} normal stress and ε_{11} strain components has demonstrated that the major part of the leading diamond facets remains under compression and in contact with the matrix when the contact force does not exceed 190 and 145 N for the Co (Figs 10a-10c) and Cu-40%Co-6%Sn (Figs 11a-11b) matrix, respectively. The area under compression dramatically decreases and the gap between the leading part of the diamond and the matrix markedly widens when the contact force increases (Figs 10d and 10c). This may promote massive crystal damage due to reflected dynamic tensile strain, exacerbated by poor contact with the matrix [2].

4. Conclusion

The effect of contact force on the magnitude of stress and strain in the surrounding matrix was studied theoretically using the finite element analysis. The results showed that, under the same loading conditions, cobalt matrix outperformed its copper-base counterpart in the load bearing capacity. This was consistent with quantitative estimates for diamond retention

acquired from granite sawing tests. Although the FEA has its limitations, because it ignores the important effects of impact loading and diamond orientation, it can be successfully used for a quick assessment of the matrix capacity for diamond retention by benchmarking against the best performing cobalt.

Acknowledgements

The authors gratefully acknowledge Professor A.S. Wronski for his invaluable comments on the manuscript. The work was funded by the Polish Ministry of Science and Higher Education through the statutory research programme.

REFERENCES

[1] J. Konstanty, Theoretical analysis of stone sawing with diamonds, J. Mater. Process. Technol. **123**, 146-154 (2002).
[2] S.W. Webb, Diamond retention in sintered cobalt bonds for stone cutting and drilling, Diamond Relat. Mater. **8**, 2043-2052 (1999).
[3] D. Tabor, The hardness of metals. The Claredon Press, Oxford, 73 (1951).
[4] D.N. Wright, H. Wapler, Investigations and prediction of diamond wear when sawing, Annals of the CIRP **35**, 1, 239-244 (1986).
[5] D.N. Wright, The prediction of diamond wear in the sawing of stone, Advances in Ultrahard Materials Application Technology, ed. C. Barrett, De Beers Industrial Diamond Division **4**, 47-60 (1988).
[6] J. Konstanty, Cobalt as a matrix in diamond impregnated tools for stone sawing applications, second ed., AGH UWND, Krakow, 2003.
[7] J. Konstanty, Diamond bonding and matrix wear mechanisms involved in circular sawing of stone, Ind. Diamond Rev. 60, 55-65 (2000).
[8] A. Romański, Doctoral Thesis, AGH, Kraków, 2000.
[9] A. Romański, J. Lachowski, Effect of friction coefficient on diamond retention capabilities in diamond impregnated tools, Archives of Metallurgy and Materials **54**, 4, 1111-1118 (2009).
[10] A. Romański, Factors affecting diamond retention in powder metallurgy diamond tools, Archives of Metallurgy and Materials **55**, 4, 1073-1081 (2010).
[11] G. Bräuninger, Production and properties of synthetic diamond grit, Proc. International Workshop on Diamond Tool Production, Turin, Italy, 3-13, November 8-10 1999.
[12] D.A. Akyüz, Doctoral Thesis, EPFL, Lausanne, 1999.
[13] Metals Handbook Vol. 2, tenth ed., ASM International, USA, 1990, pp 324, 1109.
[14] Properties of diamond, De Beers Industrial Diamond Division, Special publication K4000/5/89.
[15] S.W. Webb, W.E. Jackson, Analysis of blade forces and wear in diamond stone cutting, J. Manuf. Sci. Eng. **120**, 84-92 (1998).
[16] W. Ertingshausen, Wear processes in sawing hard stone, Ind. Diamond Rev. **45**, 254-258 (1985).
[17] Z. Feng, J.E. Field, Dynamic strengths of diamond grits, Ind. Diamond Rev. **49**, 104-108 (1989).

Received: 20 January 2014.